YTUP

Journal of Thermal Engineering

https://jten.yildiz.edu.tr/

https://doi.org/10.47481/jten.0056

RESEARCH ARTICLE

Effect of thermal energy in a four hole orifice pre combustion chamber gasoline direct injection engine: A coupled computational optimization techniques

Karthikeyan M.[1,*], Ramesh P.[2], Edward James Gunasekaran[3]

[1]Department of Mechanical Engineering, Faculty of Engineering and Technology, Annamalai University, Annamalai Nagar, 608002, India
[2]Department of Mechanical Engineering, Faculty of Engineering and Technology, Annamalai University, Annamalai Nagar, 608002, India
[3]Department of Mechanical Engineering, Faculty of Engineering and Technology, Annamalai University, Annamalai Nagar, 608002, India

Abstract

The performance and emission characteristics of a four-hole passive pre-chamber combustion (PCC) in a gasoline direct injection (GDI) engine are designed, optimized, and validated in this work. The influence of important parameters such as PCC orifice throat angle, injection pressure, and L/D ratio on engine performance is optimized using the Box-Behnken design in response surface methodology (RSM). By the utilization of RSM and CFD simulations, evaluation of performance in a GDI engine, which consists of 13 models, is done. Modelled and optimized responses are pressure, temperature, heat release rate, CO, CO_2, and NOx. CFD simulations were validated against the optimal configuration, which concludes parameters of a PCC orifice inclination of 70 degrees, an injection pressure of 65.12 bar, and an L/D ratio of 2. The findings show significant improvements in the engine performance parameters and emission reduction, NOx is reduced because of the optimal pre chamber utilization up to 23% while compare to engine without Pre chamber leading us to better insights into designing efficient and environmentally friendly combustion systems.

Keywords: Pre-Chamber Combustion, gasoline direct injection, response surface methodology, computational fluid dynamics, engine performance optimization, emission reduction

Cite this article as: Karthikeyan, M., Ramesh, P., & Gunasekaran, E. J. (2026). Effect of thermal energy in a four hole orifice pre combustion chamber gasoline direct injection engine: A coupled computational optimization techniques. Journal of Thermal Engineering, 12(5), 1665–1679. https://doi.org/10.47481/jten.0056

1. Introduction

The harmful pollutants generated by internal combustion engines, including carbon monoxide (CO), carbon dioxide (CO2), and nitrogen oxides (NOx), must be mitigated due to the enforcement of rigorous regulations by governments worldwide [1,2]. This shifts the focus of the investigation towards gasoline direct injection engines. GDI engines facilitate the direct delivery of fuel into the engine cylinder [3, 4, 5]. Particulate matter is produced in GDI engines due to the lack of proper mixture homogeneity. Consequently, it is essential to take into account the formation of mixtures within the cylinder to enhance engine efficiency [6, 7]. The implementation of pre-chamber technology enhances combustion efficiency and contributes to reduced emissions [8]. The design parameters of the pre-chamber are crucial for enhancing mixture formation, flame evolution, and optimizing flame propagation [9]. Design and analysis process of a gasoline direct injection engine with a small pre-combustion chamber created above the cylinder and was a promising approach to fulfil the specified requirements such as engine efficiency and emission reduction [10]. The use of a pre-chamber helps in enhancing the combustion process by providing a controlled and efficient ignition within the combustion chamber [11]. PCC systems play a crucial role in minimizing knock tendency, which allows for increased compression ratios that enhance thermal efficiency [12, 13]. Different orifice configurations such as orifice angles, diameter and positioning are used which creates an impact in jet forma-

*Corresponding Author
E-mail Adress: karthikbe9566@gmail.com

Submitted: 12 December 2024; **Accepted:** 9 February 2025

This paper was recommended for publication in revised form by Editor-in-Chief Ahmet Selim Dalkılıç

tion and main cylinder combustion characteristics [14, 15]. Using advances in computational fluid dynamics (CFD), the detailed analysis of PCC engines and their emission and combustion behaviors is done, which helps to optimize design parameters such as injection timing, fuel distribution, and ignition [16].

Gasoline direct injection (GDI) engines help to inject the fuel directly into the cylinder, leading to better fuel management, which improves power output and fuel efficiency [17]. But the usage of GDI engines leads to the production of NOx and particulate matter during the combustion process, which leads to the minimization of emission parameters [18, 19]. Usage of PCC in GDI systems helps in the reduction of emissions and increased combustion efficiency [20, 21]. Response surface methodology is used as an optimization tool to improve the performance of PCC-GDI engines. The utilization of CFD methods and RSM optimization combined helps to evaluate different factors that directly influence the engine performance and emission characteristics [22, 23]. The integrated methodology of RSM and CFD helps to analyze and optimize multiple factors that influence the engine performance. The interaction of factors directly influences the responses, and the understanding of the interaction of factors such as PCC orifice throat angle, injection pressure, and L/D ratio helps with the optimization of engine design [24, 25, 26]. Recent studies primarily focused on enhancing the engine performance and reducing emission characteristics in an engine [27, 28]. The integrated approach of CFD and RSM has better effectiveness to find the optimal configurations, which helps to enhance the performance parameters and to minimize CO and NOx emissions [29, 30].

This analysis aims to improve these advancements by optimizing a PCC-GDI engine using RSM and validating the results through CFD simulations. The novelty of this research work is acquiring the better PCC model while performing statistical experiments and to achieve optimized model comprising of different parameters such as orifice throat angle, injection pressure and L/D ratio.

2. Modeling and validation

The specifications of the PCC-equipped GDI engine with their operating conditions and fuel injection parameters are given in Table 1. The geometrical design process of the engine is done using CATIA V5, and geometrical data with validation is referred from literature [7]. The prepared geometrical domain underwent a surface meshing process and was checked for surface errors and rectified. Case setup was prepared for the PCC-equipped GDI engine, which consists of geometrical specifications, simulation time parameters, injector locations and orientations, boundary conditions, solver parameters, and initialized values. Selection of proper CFL limits and time step algorithm helps to enhance the simulation by handling the rapid and nonlinear dynamics. Therefore, the highly compressible flow fields during the engine combustion are improved by the use of the PISO (Pressure-Implicit splitting of operators) solver, which consists of specific convergence criteria that also help to predict the engine behavior in real time. The initialization values were provided in the initialization settings, and those are the temperature, velocity, and pressure of different regions such as the cylinder, inlet, and exhaust. The temperature in the cylinder was given to simulate realistic high-temperature conditions, which influence the combustion process and exhaust characteristics. The injector model has a 10-degree spray cone angle and a nozzle diameter of 0.0003 meters. Orientation and location of injector nozzles are important to improve fuel atomization, which controls the combustion process and reduces harmful pollutants. The injector nozzle's location and orientation are crucial parameters that control the combustion process and emission formation during combustion. Smaller diameters and optimization of spray angle help to improve the fuel atomization and reduction of particulate matter [34, 35, 36].

Table 1. Operating conditions and fuel injection parameters.

Parameter	Specifications
Bore	86mm
Stroke	86mm
Displacement	499.5cm^3
Speed	1000rpm
Valve Lift	9mm
Compression Ratio	9.2
Connecting Rod Length	145mm
Initial Pressure	101325Pa
Simulation Period	720°CA
Starting Crank Angle	-380°CA
Ending Crank Angle	+360°CA
Inlet Valve Opening	10°bTDC (Before Exhaust)
Inlet Valve Closing	55°aBDC (During Compression)
Exhaust Valve Opening	55°aBDC (During Expansion)
Exhaust Valve Closing	10°aTDC (During Suction)
Start of Injection (SOI)	-370.0° CA
Injection Duration(50, 100 and 150 Bar)	55.907° CA
Total Injected Mass	4.398e-05 Kg
Injected Species	IC8H18
Nozzle Diameter	0.0003m

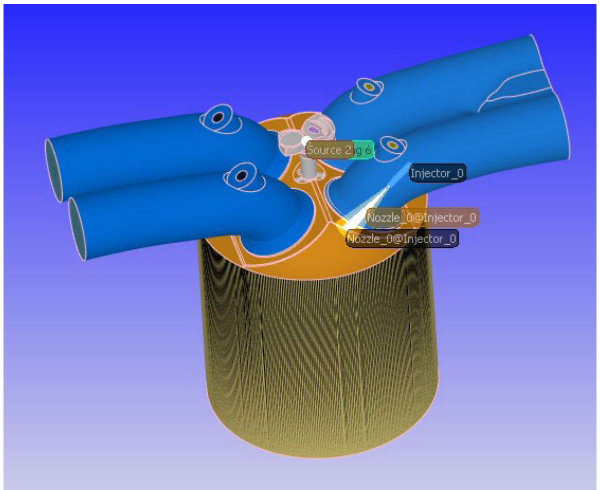

Figure 1. PCC-GDI model with separated boundaries

The layout of key components such as the fuel injector as well as the combustion chamber, which are crucial for the behavior of fuel-air mixing and to obtain efficient combustion in a PCC-GDI engine, is shown in Figure 1. The factors such as orifice throat angle, L/D ratio, and injection pressure are modified through design as shown in the figure. These factors play a vital role in engine performance during combustion and also in the emission formations. Due to the occurrence of high-speed jet flow through the pre-chamber orifice, rapid pressure and density changes happen in the main cylinder. So in order to simulate those changes, density-based solvers were used. These solvers utilize energy equations in a fully coupled manner to solve the equations, which leads to improved solution stability and helps in the handling of species transport during multiphase combustion that occurs inside the main cylinder.

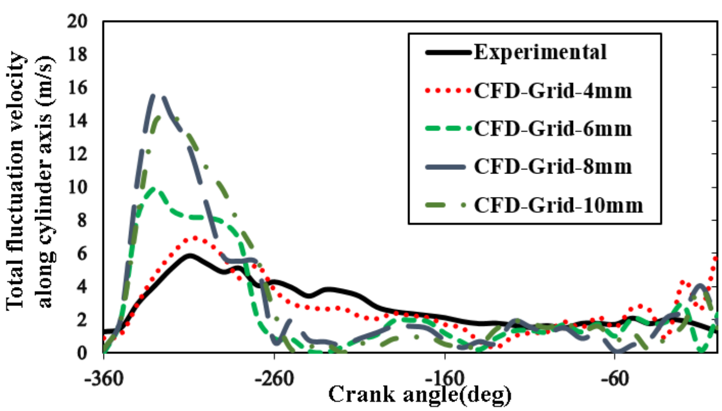

Figure 2. Grid independence study

The validation of the CFD model is done with the help of a grid independence study, which is shown in Figure 2. The analysis of grid sizes ranging from 4mm to 10mm, while 4mm grid size results are accurate and near to the experimental values. Total fluctuation in velocity around the Z-axis is calculated and compared for different grid sizes. This indicates that consideration of grid resolution is an important factor to achieve the accurate results. The impact of results varies with the finer, very fine, and coarse grids. Optimal selection of grid resolution is a crucial parameter to identify the best grid size with accurate results. Even though finer grid values lead to maximized computational time, it also comes at the cost of accurate predictions.

3. RSM analysis of CFD simulation

The factors given, such as orifice throat angle, injection pressure, and L/D ratio, and their minimum and maximum values are given as shown in Table 2. To understand the effects of factors on responses, their ranges were varied using particular minimum and maximum values. In the Box-Behnken Design (BBD), the goal is to use this range of values to systematically test and model how these factors influence the desired outcome. The method is particularly useful for optimizing the system by analyzing the main effects of each factor and their interactions.

Table 2. RSM of Box-Behnken design

S.no	Name of the factor	Minimum	Maximum
1	Orifice Throat Angle (Deg)	45	70
2	Injection Pressure (Bar)	50	150
3	L/D ratio	1	2

This study focused on finding the optimal settings of factors such as orifice angle, injection pressure, and L/D ratio to maximize performance parameters such as pressure and temperature while minimizing harmful emissions such as CO and NOx. From Table 3, it is evident that higher injection pressure values and throat angles lead to improved combustion efficiency by monitoring the results, such as higher temperatures and the formation of lower CO emissions, while the heat release rate is improved for lower L/D ratios but with increased emission formations. The purpose of the CFD is to determine the ideal combination of factors for enhancing engine performance, such as maximizing pressure and temperature while keeping emissions within acceptable limits.

Table 3. Design factors and normalized responses

Run	Surface			Normalized Response					
	Orifice Throat Angle (Deg)	Injection Pressure (Bar)	L/D Ratio	Pressure %	Temperature %	HRR %	CO %	CO_2 %	NO_x %
1	45	50	2	74.197	46.204	0.2337	78.017	21.826	87.166
2	58	100	2	91.526	51.031	15.199	88.986	9.97076	6.1291
3	70	100	2	90.785	87.212	7.8657	21.612	83.3828	11.947
4	58	100	2	91.526	51.031	15.199	88.986	9.97076	6.1291
5	70	150	2	90.56	100	0	0	100	46.968
6	45	150	2	34.312	15.312	8.7642	100	0	0
7	70	50	2	71.165	79.698	52.979	26.36	79.7305	13.122
8	70	100	1	61.391	55.809	100	16.563	87.6822	71.519
9	58	50	2	100	71.319	29.029	65.356	32.3638	44.947
10	58	150	2	93.285	61.331	26.985	80.788	15.7133	53.365
11	45	100	2	72.358	43.035	30.994	80.472	17.3321	8.5575
12	58	100	2	91.526	51.031	15.199	88.986	9.97076	6.1291
13	58	50	1	94.059	59.049	23.095	78.751	20.6753	20.744
14	58	100	2	91.526	51.031	15.199	88.986	9.97076	6.1291
15	58	150	1	63.346	37.712	7.8923	85.125	13.1583	100.02
16	45	100	1	0	0	74.871	83.912	14.3513	4.3508
17	58	100	2	91.526	51.031	15.199	88.986	9.97076	6.1291

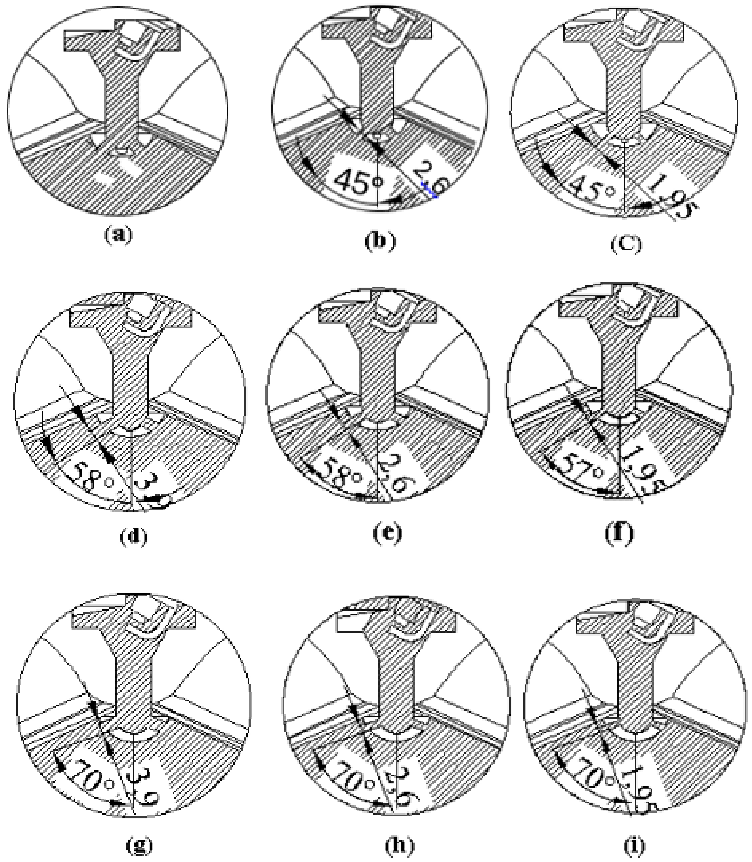

Figure 3. (a) Angle of inclination 45°, L/D ratio 1, **(b)** Angle of inclination 45°, L/D ratio 1.5, **(c)** Angle of inclination 45°, L/D ratio 2, **(d)** Angle of inclination 57.5°, L/D ratio 1, **(e)** Angle of inclination 57.5°, L/D ratio 1.5, **(f)** Angle of inclination 57.5°, L/D ratio 2, **(g)** Angle of inclination 70°, L/D ratio 1, **(h)** Angle of inclination 70°, L/D ratio 1.5, and **(i)** Angle of inclination 70°, L/D ratio 2

The centered XZ section profile of a PCC GDI engine geometry scaled at a 2:1 ratio is shown in Figure 3 (a), (b), (c), (d), (e), (f), (g), (h), and (I), based on the response surface methodology (RSM) design. The table illustrates the two key factors, namely the angle of inclination and the L/D ratio. The angles of inclination used in the CFD are 45, 57.5, and 70 degrees respectively, which represent the different geometrical configurations of the engine. Furthermore, the L/D ratio (length to diameter ratio) is varied at three levels, and the values are 1, 1.5, and 2 for each angle. This variation helps us to study how the geometry creates an impact on engine performance, such as fuel efficiency, heat release rate, and emission parameters.

4. Results and discussions

The results from the CFD analysis aid us in understanding the RSM insights and factors that impact the number of variables, such as performance parameters that consist of temperature, pressure, and heat release rate (HRR), and also for the emissions, such as CO, CO_2, and NO_x. Each response variable is analyzed statistically in order to identify the significance, as shown in Table 5. An F-value with a p-value of was obtained by modeling the pressure data using the quadratic transformation, which confirms the strong model with efficient prediction power. The model's excellent performance is confirmed by the residual sum of squares (666.72) in comparison to the entire sum of squares (10,756.92). Figure 4 shows a Box-Cox plot for six responses in order to evaluate the need for response transformation and to satisfy the assumptions of normality and constant variance. Responses such as pressure, temperature, carbon monoxide (CO), and carbon dioxide (CO_2) satisfied the regression assumptions. Logarithmic transformations are applied for responses such as heat release rate (HRR) and NOx to stabilize the variance and to enhance the predictive capability of the RSM model.

Table 5. ANOVA Table

Response (Normalized)	Source	Sum of Squares	df	Mean Square	F-value	p-value
Pressure	Quadratic model	10090.19	9	1121.13	11.77	0.0019
	Residual	666.72	7	95.25		
	Lack of Fit	666.72	3	222.24		
	Pure Error	0.0000	4	0.0000		
	Cor Total	10756.92	16			
Temperature	Linear model	7690.83	3	2563.61	22.64	< 0.0001
	Residual	1472.00	13	113.23		
	Lack of Fit	1472.00	9	163.56		
	Pure Error	0.0000	4	0.0000		
	Cor Total	9162.82	16			
HRR	Quadratic model	8.60	9	0.9555	9.52	0.0036
	Residual	0.7028	7	0.1004		
	Lack of Fit	0.7028	3	0.2343		
	Pure Error	0.0000	4	0.0000		
	Cor Total	9.30	16			
CO	Quadratic model	15254.69	9	1694.97	55.60	< 0.0001
	Residual	213.40	7	30.49		
	Lack of Fit	213.40	3	71.13		
	Pure Error	0.0000	4	0.0000		
	Cor Total	15468.09	16			
CO_2	Quadratic model	17331.35	9	1925.71	98.35	< 0.0001
	Residual	137.07	7	19.58		
	Lack of Fit	137.07	3	45.69		
	Pure Error	0.0000	4	0.0000		
	Cor Total	17468.42	16			
NO_x	Quadratic model	27.19	9	3.02	4.70	0.0268
	Residual	4.50	7	0.6428		
	Lack of Fit	4.50	3	1.50		
	Pure Error	0.0000	4	0.0000		
	Cor Total	31.69	16			

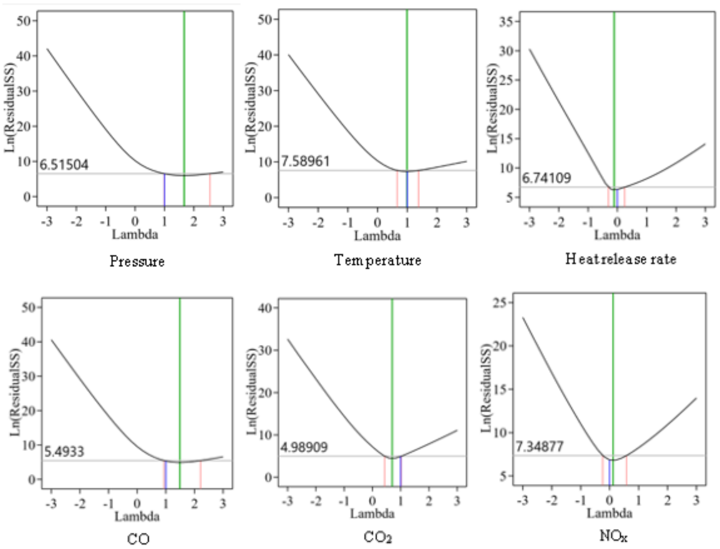

Figure 4. Box-Cox plots for six responses

As can be seen from the ANOVA findings in Table 5, a linear model was fitted for temperature. With a sum of squares of 7,690.83, this model demonstrated a substantial correlation between the input parameters and temperature results, making it highly significant ($p < 0.0001$). Figure 5 and Figure 6 show the contour plots and 3D surface analysis and demonstrate that how the L/D ratio affects temperature distribution, the ideal L/D ratio, 1.5, improves the system's temperature performance.

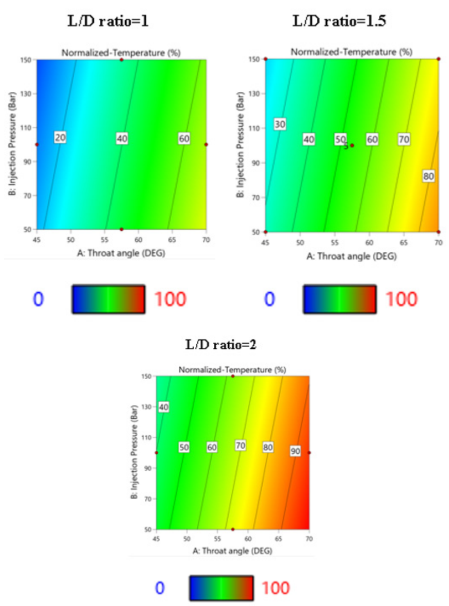

Figure 5. Combined influence of throat angle and injection pressure on temperature at different PCC L/D ratios

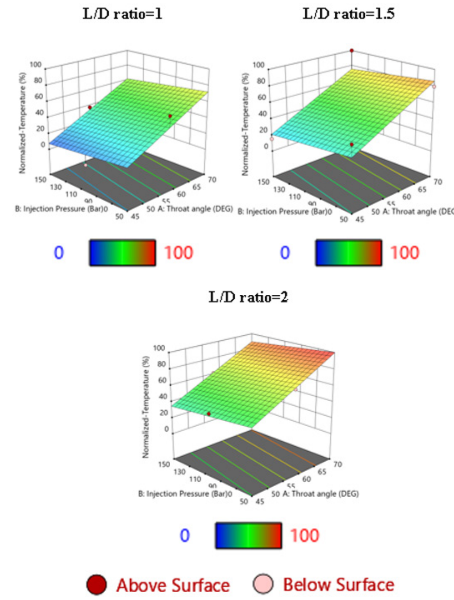

Figure 6. Interaction effect of throat angle and injection pressure on temperature at different PCC L/D ratios

According to Figure 4, the Box-Cox transformation results show that a quadratic model with a base-10 logarithmic transformation was used to analyze the HRR. Table 5 shows that this model produced a residual sum of squares of 0.70 and a significant fit ($p = 0.0036$). Using contour plots and 3D surface analysis, the HRR response is displayed, illustrating how it varies as the L/D ratio and injection pressure change, as shown in Figure 7 and Figure 8.

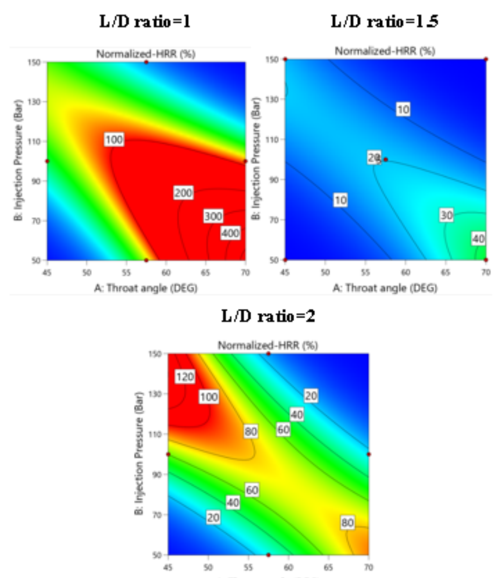

Figure 7. Heat release rate analysis of contour plots

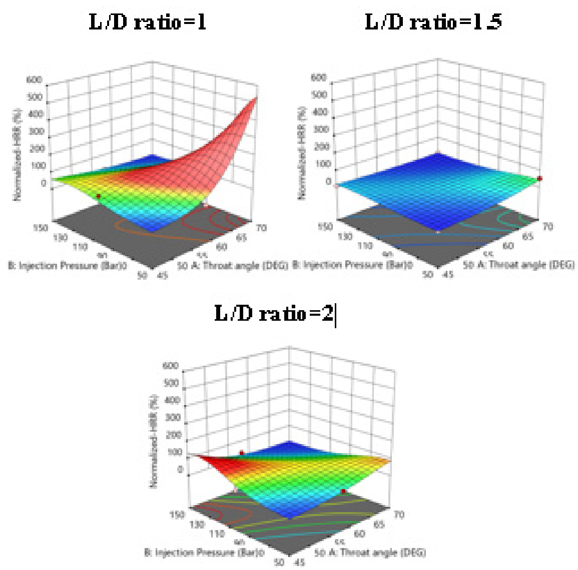

Figure 8. Heat release rate analysis of 3D surface

Emission variables, which include CO, CO2, and NOx, also followed quadratic models, whereas all the parameters yielded significant results ($p < 0.0001$ for CO and CO2, and $p = 0.0268$ for NOx), as presented in Table 5. The CO model showed particularly strong results, with an F-value of 55.60, indicating that changes in the L/D ratio and throat angle have a marked effect on CO emissions. The NOx model, which required a natural log transformation as monitored in Figure 4, demonstrated the importance of controlling temperature to minimize NOx emissions, as observed in Figure 9 and Figure 10, which present contour and 3D surface plots for NOx.

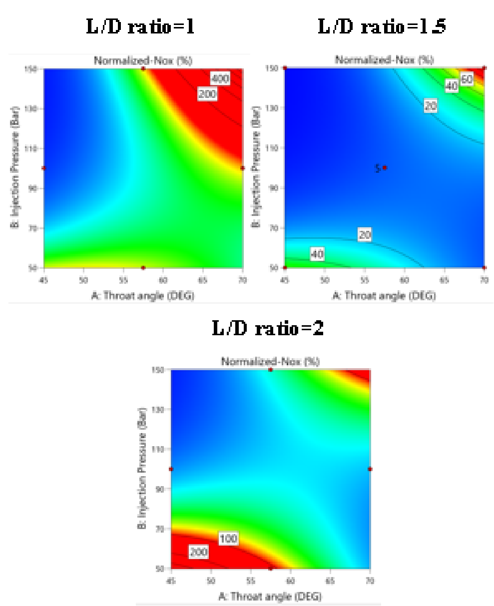

Figure 9. NO_x analysis of contour plots

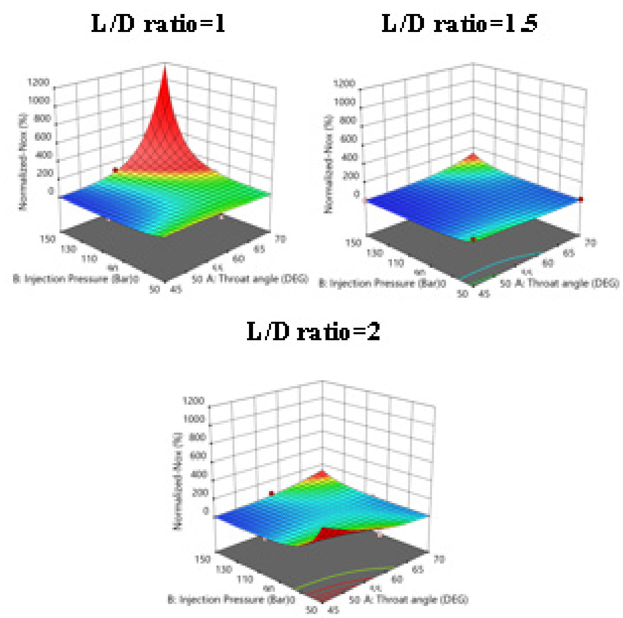

Figure 10. NO_x analysis of 3D surface

Figure 11 and Figure 12 shows the validation of performance metrics such as pressure and temperature, and as well as emission characteristics, including pollutants such as CO, CO2, and NOx. These comparisons are vital to identify whether the prediction through RSM is statistically fitted or not. This helps to assess both efficiency and impact. Any influential data points that affect the model reliability can be identified using Cook's distance, as shown in Figure 13 and Figure 14. The accuracy in the regression model is important for predicting the key outcomes. The residuals between the CFD and RSM models are plotted as shown in Figure 15, Figure 16, and Figure 17 for the performance parameters. This can be categorized into three residual types, and those are residual, internally studentized residuals, and externally studentized residuals. Each residual prediction accuracy is varied, which clearly shows how the RSM prediction model matches with the CFD models. The emission-related residual comparisons were shown in Figure 18, Figure 19, and Figure 20. Curves indicate that internally studentized and externally studentized residuals consist of deviations for every run order for the emission variables. This statistical imbalance leads to the deviations in experimental values.

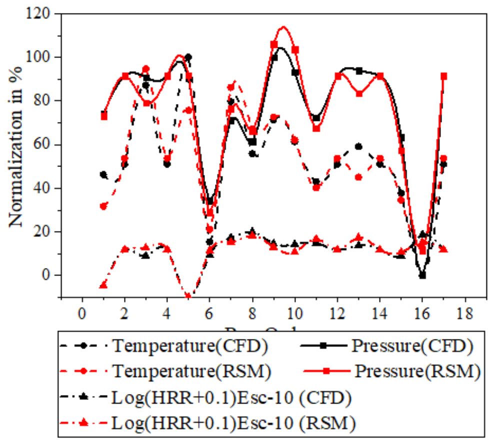

Figure 11. Validations of performance character for CFD and RSM regression model

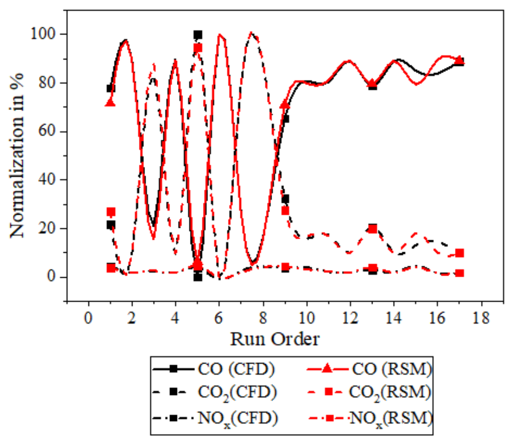

Figure 12. Validations of emission character for CFD and RSM regression model

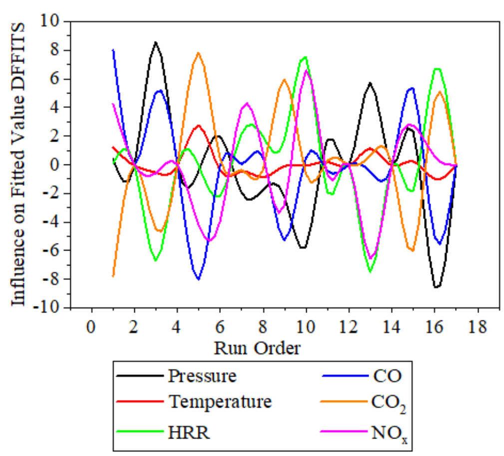

Figure 13. Statistical fit summary difference of response with run order

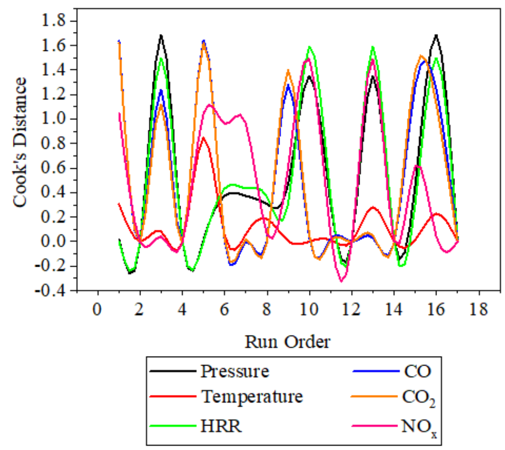

Figure 14. Analysis of regression model through cooks distance

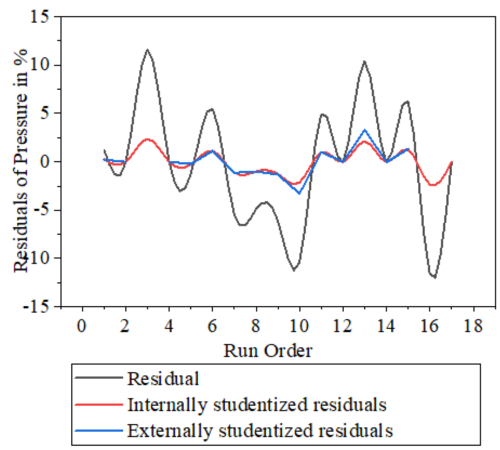

Figure 15. Pressure difference of CFD and RSM regression model

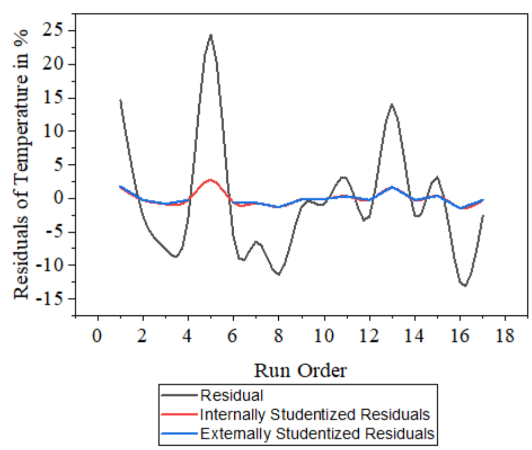

Figure 16. Temperature difference of CFD and RSM regression model

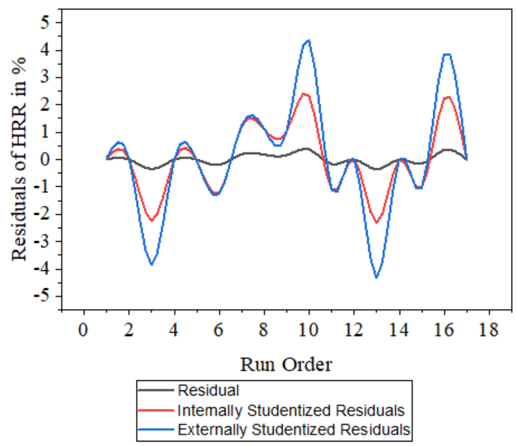

Figure 17. Heat release rate difference of CFD and RSM regression model

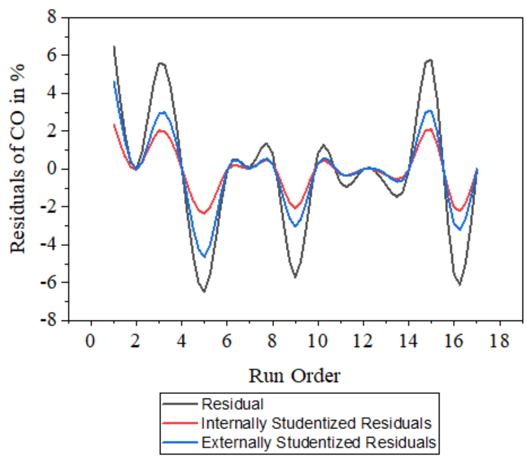

Figure 18. Carbon monoxide difference of CFD and RSM regression model

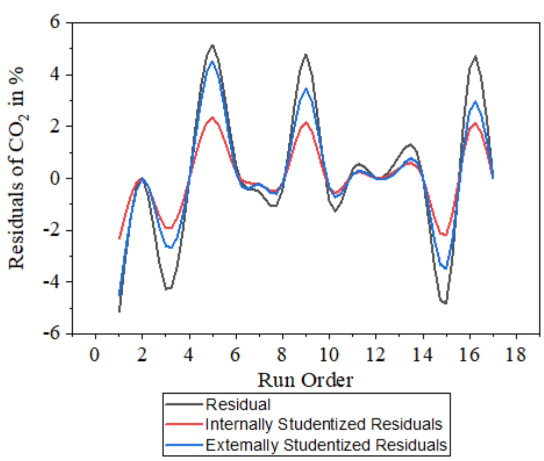

Figure 19. Carbon di oxide difference of CFD and RSM regression model

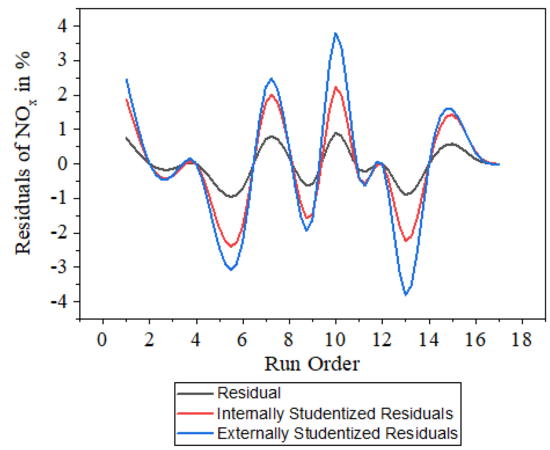

Figure 20. NO_x difference of CFD model and RSM regression model

Finally, the optimization results show that balancing emissions and combustion efficiency requires the right set of parameters. The ideal parameters are an L/D ratio of 1.945, an injection pressure of 65.12 bar, and a throat angle of 70°. These parameters minimize CO emissions to 20.07%, CO_2 to 85.341%, and NOx to 12.461%, while producing a pressure of 72.938%, a temperature of 96.831%, and an HRR of 61.453%. As indicated in Figure 21, Figure 22, and Figure 23, the optimization plots verified that these values offered the optimum balance between performance and emission reduction.

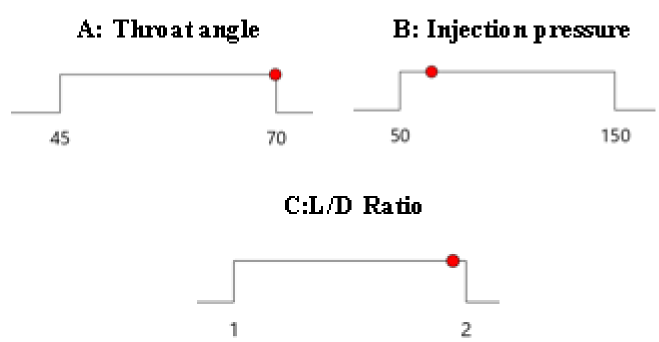

Figure 21. Optimized ramp plots for factors

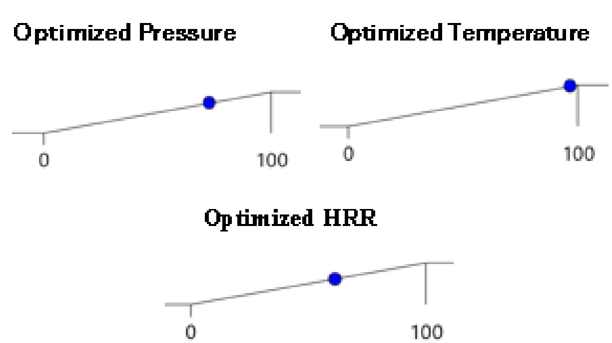

Figure 22. Optimized ramp plots for performance parameters

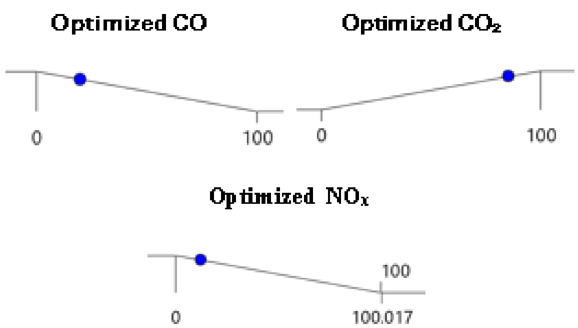

Figure 23. Optimized ramp plots for emission parameters

The fuel spray distribution inside the cylinder region was shown in Figure 24, where the design was prepared based on the optimal desired parameters. The Figure 24 shows the fuel equivalence ratio with respect to crank angle in degrees at various points during the combustion, which includes the equivalence ratio from the time of fuel injection to the time of combustion. The fuel spray timing is important to achieve a balance between power, efficiency, and emission control, which is required for an efficient and environmentally friendly combustion process. The timing of fuel injection and combustion was influenced by the crank angle. Colour indices values from Figure 24 consist of a range of values that help us identify whether the formation of the air-fuel mixture inside the cylinder is a lean or rich mixture. A ratio of 1 represents that the engine operates at stoichiometric conditions; values greater than 1 lead to a rich mixture, and less than 1 give a lean mixture. The correct fuel injection timing leads to a better air-fuel mixture formation, which enhances the combustion process.

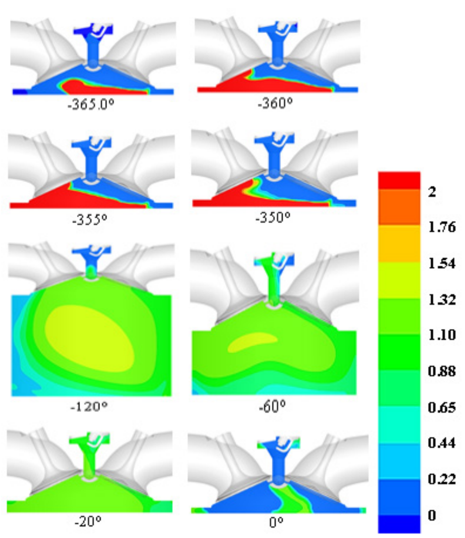

Figure 24. Fuel spray distribution of optimal desired parameter

The temperature distribution during the power stroke at different crank angles was shown in Figure 25. The observation of results highlights how the temperature varies throughout the combustion process. The distribution of temperature was observed with the aid of colour indices, which represent maximum and minimum temperature. Images from the table were taken from -20° CA to +18° CA. The temperature is higher from -4° CA to 18° CA. The progressive temperature rise is the reflection of the combustion process with higher temperatures near -6° CA, indicating the point of optimal combustion. The analysis of temperature contours shows about the spatial distribution of thermal energy inside the combustion chamber, highlighting the locations of maximum temperatures inside the cylinder during the combustion process. The temperature distribution from Figure 25 plays a vital role for a better combustion process. Achieving higher temperatures leads to an increase in pressure, which was mandatory for better combustion to take place inside the cylinder. The temperature contours from -20° CA to +20° CA indicate the flame travel and distribution from the pre-chamber to the main cylinder. Pre-chamber orifices assist flames to reach the higher velocities and distribute the high-temperature zones throughout the main cylinder regions. This results in a faster combustion process.

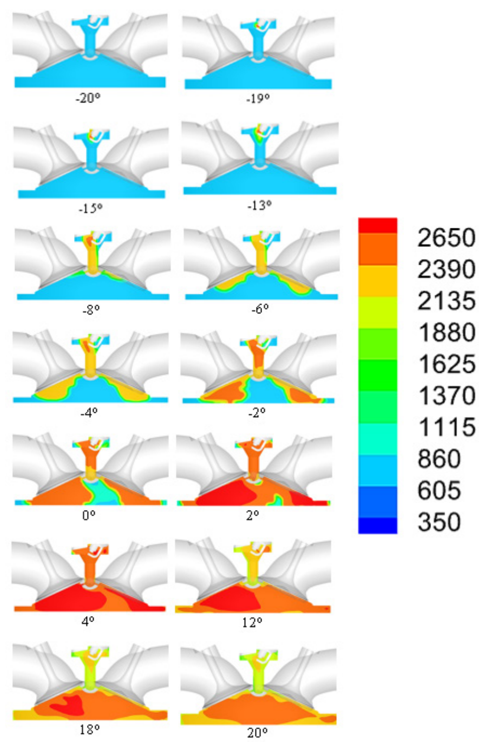

Figure 25. Temperature distribution of optimal desired parameter

The RSM model is validated afterwards in CFD to analyze the reliability and prediction of the RSM model. Figures 26, Figure 27, Figure 28, Figure 29, Figure 30, and Figure 31 shows the validation data comparisons for both the RSM model and the CFD simulation model. Performance parameters such as pressure, temperature, and heat release rate are validated. Pressure and temperature results from CFD simulations show very minor deviation when compared to the RSM model. But variable heat release rate shows major deviations, which shows the lack of prediction through RSM. Regarding the emission parameters such as CO, CO_2, and NO_x, CO and CO_2 show minor variations when compared to NO_x, which shows higher variation.

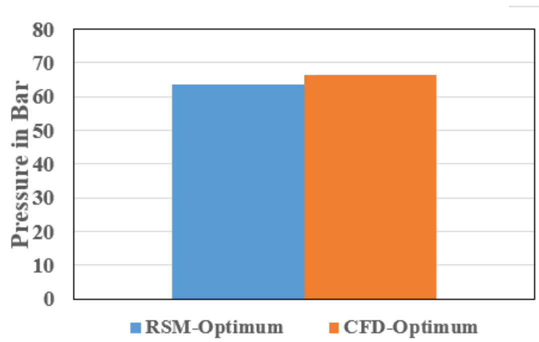

Figure 26. Validation of pressure character for RSM and CFD optimal model

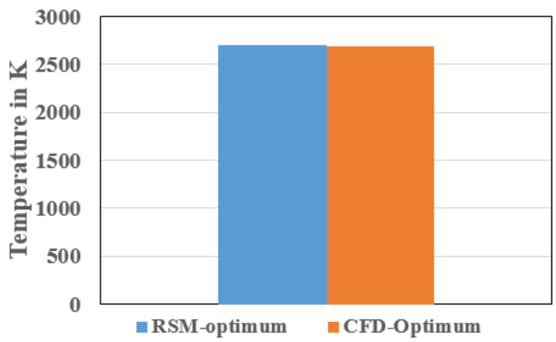

Figure 27. Validation of temperature character for RSM and CFD optimal model

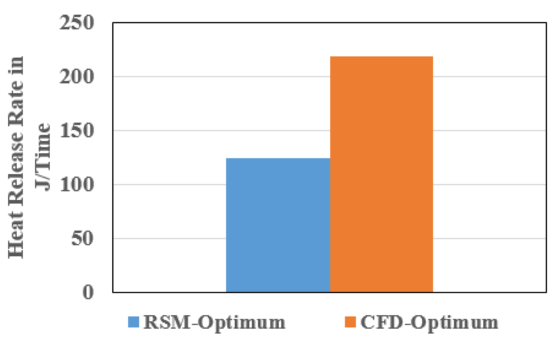

Figure 28. Validation of heat release Rate character for RSM and CFD optimal mode

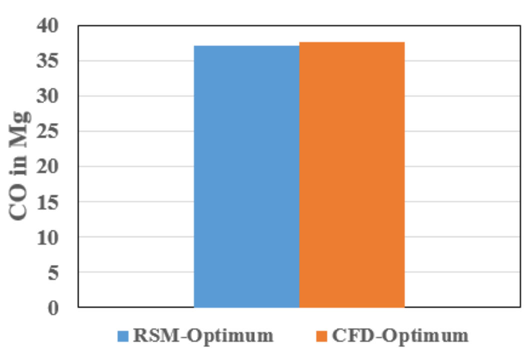

Figure 29. Validation of CO character for RSM and CFD optimal model

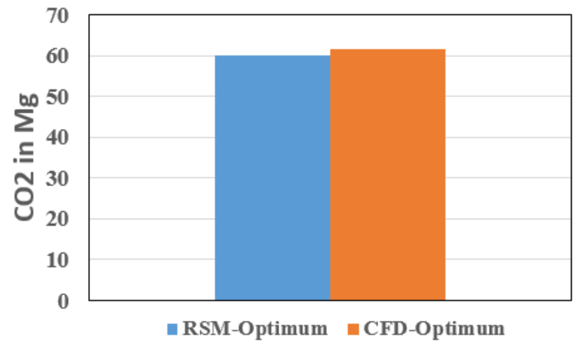

Figure 30. Validation of CO_2 character for RSM and CFD optimal mode

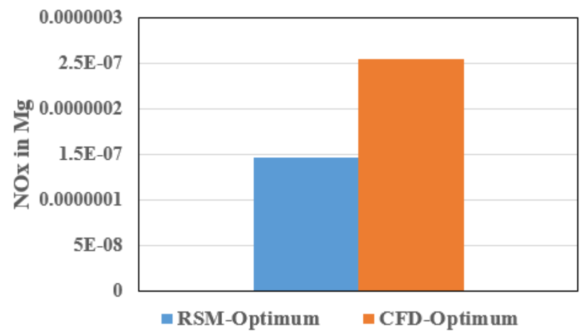

Figure 31. Validation of NO_x character for RSM and CFD optimal model

5. Conclusion

The utilization of the combined methodology of RSM and CFD in order to optimize the performance and emission characteristics of a four-hole pre-chamber combustion was successfully completed. The RSM analysis was performed by considering the factors of orifice throat angle, injection pressure, and L/D ratio to identify optimal operating ranges in order to increase the engine efficiency. The Box-Behnken design, which consists of 13 distinct models, was identified, and CFD simulations for those models were conducted, and the responses of variables are given. Analysis of variables is conducted to identify the best optimal factors, and those factors are a throat angle of 70 degrees, an injection pressure of 65.12 bar, and an L/D ratio of 1.945. Design and CFD simulation were performed for this optimal model, and the results were validated. This combined methodology of RSM and CFD together aids in minimizing harmful emissions like NOx and CO and also in order to improve the GDI engine efficiency. The refined model demonstrates improved parameters, including superior fuel-air mixing and turbulence intensity, which contribute to complete combustion. Additionally, the optimized design yields lower NOx emissions, attributed to enhanced flame propagation and minimized quenching effects. The enhancements correspond with BS VI and Euro VI emission regulations, which are pertinent for the development of low emission engines.

Author contributions statement

Karthikeyan M developed the method, performed simulations, conducted formal analysis, and wrote the original draft. Ramesh P supervised the research work, offered technical guidance, and confirmed the method. Edward James Gunasekaran aided with data analysis, interpretation of the results, and manuscript review.

Declaration of interests

The authors declare that they have no competing financial interests.

Data availability statement

The data that support the findings of this study are available from the corresponding author upon reasonable request.

Declaration of generative AI and AI-assisted technologies in the writing process

No generative AI or AI-assisted technologies were used in the writing process.

References

[1] The Ministry of Road Transport and Highways, Government of India, G.S.R. 881(E), 2019, https://morth.nic.in.

[2] Williams, M., & Minjares, R., "A technical summary of Euro 6/VI vehicle emission standards," A technical summary of Euro 6/VI vehicle emission standards, 2016, www.theicct.org.

[3] Tang, Y., Lou, D., Fang, L., Wu, X., Wang, Z. and Zhang, Y., "Research on jet ignition phases and control parameters in an active pre-chamber optical engine under ultra-lean combustion conditions," Applied thermal engineering, vol. 258, p. 124843, 2025, https://doi.org/10.1016/j.applthermaleng.2024.124843.

[4] Wang, Y., Zhang, L., Zhou, C., Guo, X., Xing, K. and Huang, H., "Numerical Study on the Potential of Stratified Mixture to Improve Thermal Efficiency and Reduce Carbon Emissions in High-Speed Gasoline Direct Injection Engine," Journal of engineering for gas turbines and power, vol. 146, no. 12, p. 121015, 2024, https://doi.org/10.1115/1.4066230.

[5] Zhang, Z., Wei, S., Chen, J., Leng, X., Zhang, S. and Ni, S., "Numerical Study of the Mixture Formation and Combustion Characteristics in Gasoline Direct Injection Engines with Conical Spray," Arabian journal for science and engineering, vol. 48, no. 9, pp. 11525-11535, 2023, https://doi.org/10.1007/s13369-022-07492-z.

[6] Sharma, N. and Agarwal, A. K., "Particulate Emission Reduction by Fuel Injection Timing Optimization in a Gasoline Direct Injection Engine," Journal of energy resources technology, vol. 144, no. 3, p. 032302, 2021, https://doi.org/10.1115/1.4051380.

[7] Singh, E., Kim, N., Vuilleumier, D., Skeen, S., Cenker, E., Sjöberg, M. and Pickett, L., " Particulate Matter Emissions in Gasoline Direct-Injection Spark-Ignition Engines: Sources, Fuel Dependency, and Quantities," Fuel, vol. 338, p. 127198, 2023, https://doi.org/10.1016/j.fuel.2022.127198.

[8] Zhao, D., An, Y., Pei, Y., Hu, J., Wang, C., Sun, Y., Xu, L., Zhang, Z. and Sun, J., "Numerical study on the inner spray and combustion of active pre-chamber jet ignition for achieving higher performance of a hybrid engine under ultra-lean conditions," Energy, vol. 309, p. 133149, 2024, https://doi.org/10.1016/j.energy.2024.133149.

[9] Lv, Y., Feng, S., Luo, J., Liu, Q., Li, L. and Kang, Z., "Effect of key structure parameters of passive pre-chamber on in-cylinder combustion processes and emissions within a gasoline engine," Case studies in thermal engineering, vol. 59, p. 104467, 2024, https://doi.org/10.1016/j.csite.2024.104467.

[10] Huang, Z., Wang, L., Pan, H., Chen, H., Li, J., Wang, T., & Wang, L., "Effects of key parameters of pre-chamber on engine combustion and emissions," Thermal Science and Engineering Progress, vol. 49, pp. 102450, 2024, https://doi.org/10.1016/j.tsep.2024.102450.

[11] Tomić, R., Sjerić, M., Krajnović, J., & Ugrinić, S., "Influence of Pre-Chamber Volume, Orifice Diameter and Orifice Number on Performance of Pre-Chamber SI Engine—An Experimental and Numerical Study," Energies, vol. 16, no. 6, pp. 2884, 2023, https://doi.org/10.3390/en16062884.

[12] Duan, W., Huang, Z., Chen, H., Tang, P., Wang, L., & Chen, W., "Effects of passive pre-chamber jet ignition on combustion and emission at gasoline engine," Advances in Mechanical Engineering, vol. 13, no. 12, p. 10, 2021, https://doi.org/10.1177/16878140211067148.

[13] Santos, N. D., dos Santos, I. R., Roso, V. R., Alvarez, C. E., & Baeta, J. G., "Knock metrics experimental evaluation for pre-chamber SI engines,"Proceedings of the Institution of Mechanical Engineers, vol. 238, no. 9, pp. 2865-2879, 2024, https://doi.org/10.1177/09544070231171963.

[14] Basha, K. B. J., Balasubramani, S. & Sivasankaralingam, V., " An experimental study on the influence of nozzle hole numbers and patterns of a passive pre-chamber spark ignition system," International Journal of Hydrogen Energy, vol. 91, pp. 1207-1220, 2024, https://doi.org/10.1016/j.ijhydene.2024.10.226.

[15] Huang, L., Tang, Q., Sun, J., Zhu, X. and Yao, M., "Computational study of the impacts of the nozzle configurations on passive pre-chamber engine combustion," Applied thermal engineering, vol. 250, no. 123530, 2024, https://doi.org/10.1016/j.applthermaleng.2024.123530.

[16] Ramesh, P., & Gunasekaran, E. J., "Emission Reduction in a GDI Engine with Different Injection Timings – A CFD Investigation," International review on modelling and simulations (IREMOS), vol. 7, no. 4, pp. 729-739, 2014, https://doi.org/10.15866/iremos.v7i4.2941.

[17] Addepalli, S. K., & Mallikarjuna, J. M., “Modelling Ignition and Combustion in GDI Engines,” In P. A. Lakshminarayanan, A. K. Agarwal, H. Ge, & J. M. Mallikarjuna (Eds.), Modelling Spark Ignition Combustion, pp. 241-300, 2024, https:/doi.org/10.1007/978-981-97-0629-7_7.

[18] Yan, Y., Yang, R., Sun, X., Li, R., & Liu, Z., “Numerical Investigations of Injection Timing Effects on a Gasoline Direct Injection Engine Performance: Part A, In-Cylinder Combustion Process,” Frontiers in energy research, vol. 10, no. 828167, 2022, https://doi.org/10.3389/fenrg.2022.828167.

[19] Li, X., Liu, S., Li, W., Pei, Y., Zhang, X., Ni, P., . . . Wang, C., “Optimising the Particulate Emission Characteristics of a Dual-Fuel Spark Ignition Engine by Changing the Gasoline Direct Injection Strategy,” Sustainability, vol. 16, no. 19, p. 8713, 2024, https://doi.org/10.3390/su16198713.

[20] Stangierska, M., Bajwa, A., Lewis, A., Akehurst, S., Turner, J., & Leach, F., “Ensemble Machine Learning Techniques for Particulate Emissions Estimation from a Highly Boosted GDI Engine Fuelled by Different Gasoline Blends,” Energy & Propulsion Conference & Exhibition, vol. 7, no. 4, pp. 1647-1663, 2024, https://doi.org/10.4271/2024-01-4306.

[21] Muthukumar, S., Gunasekaran, E. J., Ramesh, P. and Karthikeyan, M., “Numerical investigation of a GDI engine with pre-combustion Chamber,” International Journal of Advanced Technology and Engineering Exploration, vol. 10, no. 106, pp. 1242-1259, 2023, https://doi.org/10.19101/IJATEE.2022.10100290.

[22] Yin, C., Zhu, M., Zhao, X., & Zhang, Z., “Experimental and simulation study on lean combustion characteristics of passive pre-combustion chamber ignition boosted GDI engine,” Proceedings of the Institution of Mechanical Engineers, vol. 239, no. 4, pp. 1676-1690, 2025, https://doi.org/10.1177/09544070241277933.

[23] Palani, T., Esakkimuthu, G. S., Dhamodaran, G. and Sundaraganesan, A., “Performance optimization of gasoline engine fuelled with ethanol/n-butanol/gasoline blends using response surface methodology,” Biofuels, vol. 15, no. 1, pp. 33-45, 2024, https://doi.org/10.1080/17597269.2023.2215631.

[24] Bharath, B. K., & Selvan, V. A., “Optimizing Spark-Ignition Engine Performance with Ternary Blend Fuels and Hybrid Nanolubricants: A Response Surface Methodology Study,” SAE Int. J. Engines, vol. 17, no. 8, pp. 1017-1047, 2024, https://doi.org/10.4271/03-17-08-0059.

[25] Elumalai, R., Ravi, K., Elumalai, P. V., Sreenivasa Reddy, M., Prakash, E., & Sekar, P., “ Development of an ammonia-biodiesel dual fuel combustion engine’s injection strategy map using response surface optimization and artificial neural network prediction.,” Scientific reports, vol. 14, no. 1, p. 543, 2024, https://doi.org/10.1038/s41598-023-51023-1.

[26] Ahmad, A., Yadav, A. K., & Hasan, S., “Enhanced production of methane enriched biogas through intensified co-digestion process and its effective utilization in a biodiesel/biohydrogen fueled engine with duel injection strategies: ML-RSM based an efficient optimization approach,” International Journal of Hydrogen Energy, vol. 65, pp. 671-686, 2024, https://doi.org/10.1016/j.ijhydene.2024.04.059.

[27] Ahmad, A., & Singh, A., “Predictive Modeling and Optimization of Engine Characteristics with Biogas-Biodiesel-Powered Dual-Fuel Mode: A Neural Network-Coupled Box-Behnken Design,” Arabian Journal for Science and Engineering, vol. 49, no. 2, pp. 2661-2680, 2024, https://doi.org/10.1007/s13369-023-08375-7.

[28] Yu, T., Lee, D. E., Gore, J. P., & Qiao, L., “Gas-Dynamic Interactions between Pre-Chamber and Main Chamber in Passive Pre-Chamber Ignition Gasoline Engines,” SAE International Journal of Engines, vol. 17, no. 1, pp. 135-149, 2024, https://doi.org/10.4271/03-17-01-0008.

[29] Wang, R., Zhou, F., Liu, J., Zhang, Q., Qiao, J., Jia, D., . . . Shen, D., “Experimental investigation of the influence of pre-chamber structural parameters on combustion and emission characteristics of a high compression ratio SI engine,” Thermal Science and Engineering Progress, vol. 47, no. 102318, 2024, https://doi.org/10.1016/j.tsep.2023.102318.

[30] Sivakumar, D. B., Arulmozhi, M., Sathyanarayanan, S., & Sridharan, M., “Optimization of gasoline engine operating parameters fueled with DIPE-gasoline blend: Comparative evaluation between response surface methodology and fuzzy logic expert system,” Process Safety and Environmental Protection, vol. 158, pp. 291-307, 2022, https://doi.org/10.1016/j.psep.2021.12.015.

[31] Yaman, H., Yesilyurt, M. K., & Uslu, S., “Simultaneous optimization of multiple engine parameters of a 1-heptanol / gasoline fuel blends operated a port-fuel injection spark-ignition engine using response surface methodology approach,” Energy, vol. 238, no. 122019, 2022, https://doi.org/10.1016/j.energy.2021.122019.

[32] Sim, J., Chang, J., & Badra, J., “CFD-guided optimization of the injector and injection parameters for light-duty GCI engine,” Fuel, vol. 316, no. 123389, 2022, https://doi.org/10.1016/j.fuel.2022.123389.

[33] Jin, W., Gan, H., Cong, Y., & Li, G., “ Performance Optimization and Knock Investigation of Marine Two-Stroke Pre-Mixed Dual-Fuel Engine Based on RSM and MOPSO,” Journal of Marine Science and Engineering, vol. 10, no. 10, p. 1409, 2022, https://doi.org/10.3390/jmse10101409.

[34] Uslu, S., Yaman, H., & Yesilyurt, M. K., “Optimization of Parameters Affecting the Performance and Emissions of a Spark Ignition Engine Fueled with n-Pentanol/Gasoline Blends Using Taguchi Method,” Arabian Journal for Science and Engineering, vol. 46, no. 11, pp. 11711-11724, 2021, https://doi.org/10.1007/s13369-021-05675-8.

[35] Li, X., Li, D., Pei, Y., & Peng, Z., “ Optimising microscopic spray characteristics and particle emissions in a dual-injection spark ignition (SI) engine by changing GDI injection pressure,” International Journal of Engine Research, vol. 24, no. 4, pp. 1290-1299, 2023, https://doi.org/10.1177/14680874221082793.

[36] Hu, C., Wu, Z., Ferrari, A., Ji, M., Deng, J., & Vento, O., "Numerical Study on Internal Flow and Cavitation Characteristics of GDI Injectors for Different Nozzle Orifice Geometries," Energies, vol. 17, no. 16, Art. No. 4114, 2024, https://doi.org/10.3390/en17164114.